Nonpolar and semipolar InGaN/GaN multiple-quantum-well solar cells with improved carrier collection efficiency

Xuanqi Huang, , Houqiang Fu, , Hong Chen, , Xiaodong Zhang, , Zhijian Lu, , Jossue Montes, , Michael Iza, , Steven P. DenBaars, , Shuji Nakamura, and , and Yuji Zhao

Citation: Appl. Phys. Lett. **110**, 161105 (2017); doi: 10.1063/1.4980139
View online: http://dx.doi.org/10.1063/1.4980139
View Table of Contents: http://aip.scitation.org/toc/apl/110/16
Published by the American Institute of Physics

Nonpolar and semipolar InGaN/GaN multiple-quantum-well solar cells with improved carrier collection efficiency

Xuanqi Huang,[1] Houqiang Fu,[1] Hong Chen,[1] Xiaodong Zhang,[1] Zhijian Lu,[1] Jossue Montes,[1] Michael Iza,[2] Steven P. DenBaars,[2] Shuji Nakamura,[2] and Yuji Zhao[1,a)]
[1]*School of Electrical, Computer & Energy Engineering, Arizona State University, Tempe, Arizona 85287, USA*
[2]*Materials Department, University of California, Santa Barbara, California 93106, USA*

(Received 19 December 2016; accepted 3 April 2017; published online 17 April 2017)

We demonstrate the nonpolar and semipolar InGaN/GaN multiple-quantum-well (MQW) solar cells grown on the nonpolar *m*-plane and semipolar $(20\bar{2}1)$ plane bulk GaN substrates. The optical properties and photovoltaic performance of the nonpolar and semipolar InGaN solar cells were systematically studied, and the results were compared to the conventional polar *c*-plane devices. The absorption spectra, current density–voltage (J–V) characteristics, external quantum efficiency (EQE), and internal quantum efficiency (IQE) were measured for nonpolar *m*-plane, semipolar $(20\bar{2}1)$ plane, and polar *c*-plane InGaN/GaN MQW solar cells. Nonpolar *m*-plane InGaN/GaN MQW solar cells showed the best performance across all devices, with a high open-circuit voltage of 2.32 V, a low bandgap-voltage offset of 0.59 V, and the highest EQE and IQE. In contrast, the polar *c*-plane device showed the lowest EQE despite the highest absorption spectra. This huge difference is attributed to the better carrier transport and collection on nonpolar *m*-plane devices due to the reduced polarization effects, which were further confirmed by bias-dependent EQE measurements and energy band diagram simulations. This study demonstrates the high potential of nonpolar and semipolar InGaN solar cells and can serve as guidance for the future design and fabrication of high efficiency III-nitride solar cells. *Published by AIP Publishing.*
[http://dx.doi.org/10.1063/1.4980139]

Recent years have seen an increasing interest in the development of III-nitride InGaN solar cells. This interest has been driven by the favorable physical properties of III-nitrides for photovoltaic applications such as strong absorption coefficients (on the order of $10^5\,cm^{-1}$ near the band edge), tunable bandgap from 0.70 eV to 3.4 eV, outstanding thermal performance,[1–4] and superior radiation resistance under harsh environments.[5] The InGaN solar cell is therefore a promising candidate for future high-efficiency thin film photovoltaic (PV) applications, especially for the fabrication of top cells in ultra-high-efficiency multi-junction solar cells (e.g., >50%) and for space and terrestrial concentrated PV applications. There have been increasing reports on the InGaN solar cells, and their PV performance and conversion efficiency were steadily improved.[6–13] For example, Neufeld *et al.* demonstrated an InGaN/GaN p-i-n double heterostructure solar cell with the 200 nm InGaN active layer.[6] This solar cell showed a short circuit current density (J_{sc}) of $4.2\,mA/cm^2$ and open circuit voltage (V_{oc}) of 1.81 V under AM0 illumination. Recently, it was realized that the performance of InGaN solar cell devices can be further improved by utilizing strained InGaN quantum wells (QWs) or superlattice active layer structures,[8,14] which are similar to the device designs of commercial light-emitting diodes (LEDs). Kuwahara *et al.* at Nagoya University showed an InGaN-based superlattice solar cell with a high J_{sc} of $3.08\,mA/cm^2$ and a high fill factor (FF) of 70% under AM1.5G 1.5 suns condition. Consequently, the high performance InGaN QW solar cells with high V_{oc} of >2.0 V, high EQE of >40%, and high FF of >50% have been achieved in the following reports.[6–12] Therefore, recent developments of InGaN solar cells have benefited from the comprehensive research efforts in other III-nitride optoelectronic devices[15–24] such as light-emitting diodes (LEDs)[15–18] and laser diodes (LDs)[15,20,21,25] where InGaN/GaN multiple-quantum-well (MQW) structures are now being widely utilized for developing high-efficiency III-nitride solar cells[4,7,9,10,26,27] Despite the encouraging progress, the performance of current InGaN solar cells is still unsatisfactory, especially when compared with well-developed PV devices based on Si or III-V materials. For instance, the typical conversion efficiency of mature 1J GaAs solar cell is more than 20%. In comparison, it is still lower than 5% for 1J InGaN solar cell despite high EQE and IQE values, which is mainly due to the narrow absorption spectrum. Therefore, considerable materials and device challenges still need to be addressed before the full potential of InGaN solar cells can be realized.

One critical challenge to the development of high performance InGaN solar cells arises from the polarization-related effects that exist in conventional InGaN solar cells grown on polar *c*-plane substrates.[9,10,26] The discontinuities in both spontaneous and piezoelectric polarization at the *c*-axis InGaN/GaN heterointerface will lead to large internal electric fields inside the QWs, which is detrimental to the device performance.[28–31] For LED devices, it was well observed that the polarization-related effects will lead to reduced electron-hole wavefunction overlap, reduced radiative recombination rate, and reduced device efficiency.[17,32] For solar cell devices, it was recently demonstrated that the same effects will also adversely affect the solar cells where

a)Yuji.Zhao@asu.edu

the polarization-related electric fields will inhibit the transport of photogenerated carriers and thus dramatically reduce the collection and conversion efficiency of solar cells.[28,29,31] Although circumventive methods such as polarization doping have been proposed (e.g., inserting heavily doped p and n GaN layers on each side of the QWs),[33] these results are less satisfactory as it is difficult to control the doping profile and the short-circuit current can be reduced due to the high resistivity of p-GaN layers. Therefore, innovative approaches in materials and device engineering must be sought.

Alternatively, growth of InGaN solar cells along the nonpolar and semipolar orientations offers an attractive approach to address the polarization-related effects. It has been already shown in III-nitride LEDs that nonpolar and semipolar devices will have eliminated or reduced polarization-related effects and therefore much improved device performance.[16,34,35] Furthermore, other advantageous features such as reduced defect densities from bulk substrates, improved In incorporation, more uniform alloy composition in QWs have also been reported on nonpolar and semipolar materials,[15,32,36] which may be beneficial for developing high efficient InGaN solar cells. Despite these appealing material properties, there is still no systematic study on InGaN solar cells based on nonpolar or semipolar III-nitrides, and their detailed device performance is still unknown. In this work, we fabricate and characterize InGaN/GaN MQW solar cells grown on the nonpolar *m*-plane, semipolar $(20\bar{2}1)$ plane, and polar *c*-plane bulk GaN substrates. The absorption spectra, current density–voltage (J–V) characteristics, external quantum efficiency (EQE), and internal quantum efficiency (IQE) were measured for those devices. The solar cell performance showed a strong dependence on the polarization-related effects, where nonpolar *m*-plane solar cells exhibited the best PV performance due to the eliminated polarization effects, which were further confirmed by bias-dependent EQE measurements and energy band diagram simulations.

InGaN/GaN MQW solar cells were grown by conventional metal-organic chemical vapor deposition (MOCVD) on the nonpolar *m*-plane, semipolar $(20\bar{2}1)$ plane, and polar *c*-plane GaN substrates. All the samples have the same device structures where the MOCVD growth conditions were carefully adjusted to achieve In compositions of ~20% in the QWs. The device structure consists of 1 μm Si-doped n-GaN ([Si]=5 $\times 10^{18}$ cm^{-3}), 10 nm highly Si-doped n$^+$-GaN ([Si]=1 $\times 10^{19}$ cm^{-3}), 20 periods of InGaN (6 nm)/GaN (10 nm) MQWs, 30 nm Mg-doped smooth p$^+$-GaN ([Mg]=1 $\times 10^{19}$ cm^{-3}), 120 nm Mg-doped intentionally roughened p-GaN ([Mg]=3 $\times 10^{19}$ cm^{-3}), and the 10 nm highly Mg-doped p$^+$-GaN contact layer ([Mg]=1 $\times 10^{20}$ cm^{-3}). The schematic device structure is shown in the inset of Fig. 1. Material characterizations such as high resolution x-ray diffraction (HRXRD) analysis and atomic force microscopy were performed (data not shown here), which revealed similar material properties of all the samples in terms of alloy composition and surface roughness. The transmission and reflectance spectra of the samples were measured using LAMBDA 950/1050 UV/VIS/NIR Spectrophotometer from Perkin Elmer, and then, absorption spectra were determined from $A(\lambda) = 1 - T(\lambda) - R(\lambda)$. The samples were then fabricated into 1 mm × 1 mm mesas by standard contact lithography and inductively coupled plasma (ICP) etching. Ti/Al/Ni/Au n-type contacts were deposited around the perimeter of the mesa, and Ni/Au p-type grid contacts with a center-to-center grid spacing of 200 μm were deposited via electron beam evaporation. The fabricated solar cell devices were characterized by illuminated J–V measurements with a Keithley 2420 source meter under an Oriel Class A Solar Simulator with AM1.5G and 1 sun condition. EQE measurement data were collected using a 150W Xenon arc lamp coupled with a Cornerstone 260 1/4 m monochromator and calibrated with a reference Si photodetector. Energy band diagrams were simulated using SiLENSe, developed by STR Group.[37]

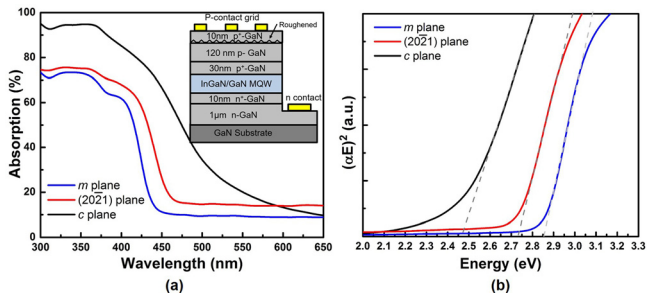

FIG. 1. (a) Room temperature transmission spectra and (b) Tauc's plots of *m*-plane, $(20\bar{2}1)$ plane, and *c*-plane InGaN MQW solar cells. The inset shows the cross-section schematic structure of the MQW InGaN solar cells.

Figure 1(a) presents the absorption spectra of InGaN/GaN MQW solar cell samples on the nonpolar *m*-plane, semipolar $(20\bar{2}1)$ plane, and polar *c*-plane GaN substrates. The results show that the absorption cutoff wavelength of the devices redshifts with increasing polarizations inside the materials, i.e., *c*-plane > $(20\bar{2}1)$ plane > *m*-plane. This indicates a smaller effective bandgap in *c*-plane InGaN solar cells possibly due to a larger QW tilting caused by stronger polarization-related effects.[38] Figure 1(b) shows Tauc's plots for all the samples. The effective bandgap energies (E_g) are 2.85 eV, 2.73 eV, and 2.45 eV for *m*-plane, $(20\bar{2}1)$ plane, and *c*-plane samples, respectively. Furthermore, it was also observed that the absorption edge tends to broaden with increasing polarization of the devices, which can be characterized by the Urbach tail energy (E_u). E_u is strongly related to the band structures.[39,40] In this case, this broadening of absorption edge can be attributed to the different band structures, e.g., valence band states,[41] due to different polarities of the GaN substrates. In the meantime, it is also believed that increasing material defects can also lead to the broadening of the absorption edge. This trend is also in a good agreement with our previous theoretical analysis, which suggests that E_u can modify the effective bandgap energy, thus affecting the optical properties and device performance of the solar cells.[42]

Figure 2 shows (a) illuminated J–V curves, (b) EQE spectra under zero bias, and (c) IQE spectra for the fabricated nonpolar *m*-plane, semipolar $(20\bar{2}1)$ plane, and polar *c*-plane InGaN/GaN MQW solar cells. Table I summarizes the key device parameters, including the values of E_g from Tauc's plots, V_{oc}, bandgap-voltage offset (W_{oc}), J_{sc}, FF, EQE, and IQE for all the devices. The IQE is defined as the ratio of EQE and absorption spectra: $IQE = EQE/absorption$, which is a fine gauge of carrier collection efficiency. The bandgap-voltage offset W_{oc} is defined as the difference between the effective bandgap and V_{oc}, which is an indicator of quasi-

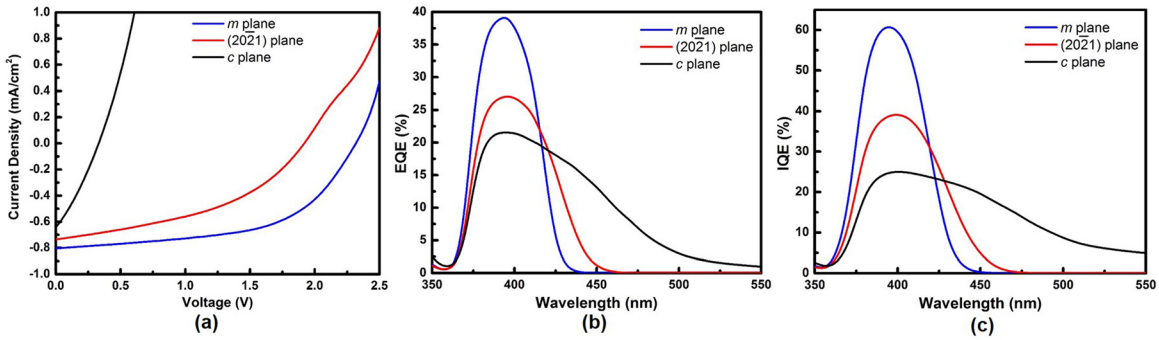

FIG. 2. (a) Illuminated J–V curves for *m*-plane, (20$\bar{2}$1) plane, *c*-plane, InGaN MQW solar cells. (b) EQE and (c) IQE curves for *m*-plane, (20$\bar{2}$1) plane, *c*-plane InGaN MQW solar cells.

TABLE I. Summary of key device parameters for nonpolar *m*-plane, semipolar (20$\bar{2}$1) plane, and polar *c*-plane InGaN/GaN MQW solar cell devices.

	E_g (eV)	V_{oc} (V)	W_{oc} (V)	J_{sc} (mA/cm^2)	FF (%)	Peak EQE (%)	Peak IQE (%)
m-plane	2.85	2.32	0.53	0.803	55.5	39.4	61.4
(20$\bar{2}$1) plane	2.73	1.92	0.81	0.736	43.2	27.1	39.6
c-plane	2.45	0.33	…	0.644	29.9	21.5	25.2

Fermi level splitting at the open circuit condition.[43] Nonpolar *m*-plane solar cell device showed the smallest W_{oc} value compared to other devices. Furthermore, it showed the best device performance, with a V_{oc} of 2.32 V, W_{oc} of 0.59 V, J_{sc} of 0.803 mA/cm^2, FF of 55.5%, and peak EQE of 39.4%. Compared to the previously reported nonpolar InGaN solar cell device on *r*-plane sapphire,[44] our nonpolar device presents a much higher V_{oc}. Although polar *c*-plane solar cell initially showed the highest absorption in the optical measurement [Fig. 1(a)], it showed lower EQE and IQE when compared to nonpolar and semipolar (20$\bar{2}$1) devices. This result is possibly due to the strongest polarization-related effects on polar *c*-plane devices, which resulted in a poor carrier transport and collection in the electric measurement. This is also evident from the low J_{sc} on the polar *c*-plane devices. The short circuit current J_{sc} can be approximated by the equation

$$J_{sc} = \int_0^\infty qF(\lambda) \times EQE(\lambda) d\lambda = \int_0^\infty qF(\lambda) \times IQE(\lambda) \times absorption(\lambda) d\lambda, \quad (1)$$

where $F(\lambda)$ is the photon flux of the given solar spectrum. It can be seen that J_{sc} is proportional to EQE, which is the product of IQE and absorption. Although the absorption spectra of *c*-plane solar cell are much higher than nonpolar and semipolar devices, the poor carrier collection efficiency, represented by IQE, leads to a very low J_{sc} and poor PV performance. Conversely, the nonpolar *m*-plane and semipolar (20$\bar{2}$1) solar cells showed higher EQE despite the lower absorption than that of the polar *c*-plane device, which can be attributed to improved carrier collection efficiency from reduced polarization-related effect. This result suggests that the polarization-related effects will significantly impact the carrier collection efficiency and the PV performance of III-nitride InGaN solar cells. The light J–V and EQE results presented here are also consistent with previous simulation results, which indicates that high polarization charges will change the band diagram profiles of InGaN solar cells and thus lead to reduced short-circuit currents.[28] Overall, the performance of nonpolar and semipolar InGaN solar cells is comparable to the previous reports of III-nitride solar cells. Further PV performance improvements can be expected with more advanced devices structures such as thicker absorption layers,[10,45] thinner GaN barriers,[11,46,47] and better optical designs.[11,48,49]

To further investigate the effect of the polarization field on carrier transport on InGaN MQW solar cells, the EQEs of nonpolar *m*-plane, and semipolar (20$\bar{2}$1) plane, and polar *c*-plane MQW solar cells were measured under different negative bias, and the results were presented in Figs. 3(a)–3(c). In order to better quantify the difference in EQEs under different bias, the relative EQE was plotted where the EQE spectra from zero bias to −4 V reverse bias were normalized using the peak EQE value under the zero condition. For the polar *c*-plane solar cell, the ratio of peak EQE under −4 V reverse bias and zero bias is as large as ∼7, while the ratios are only ∼1.60 and ∼1.23 for the semipolar (20$\bar{2}$1) plane device and the nonpolar *m*-plane, respectively. The high ratio of EQEs under negative/zero bias on polar *c*-plane solar cells is consistent with previous reports and was attributed to the large polarization-related effects.[33] The large polarization field on polar *c*-plane structures creates higher barrier between the QWs, thus affecting carrier tunneling and transporting, which will lead to reduced carrier collection efficiency of the solar cells under zero bias. The applied negative bias will screen and partially offset the polarization-induced electric field, and enhance the carrier transport and collection in the QWs, leading to an increased EQE for the solar cells under negative bias. On the other hand, the small difference in EQEs under zero/negative bias on nonpolar and semipolar (20$\bar{2}$1) solar cells clearly indicates the much smaller polarization-related effects in these devices and is consistent with previous EQE results. In addition, it can also be observed that for the polar *c*-plane solar cell, the absorption edge or the cutoff wavelength of EQE spectra increases when the applied negative bias increases, indicating a strong change

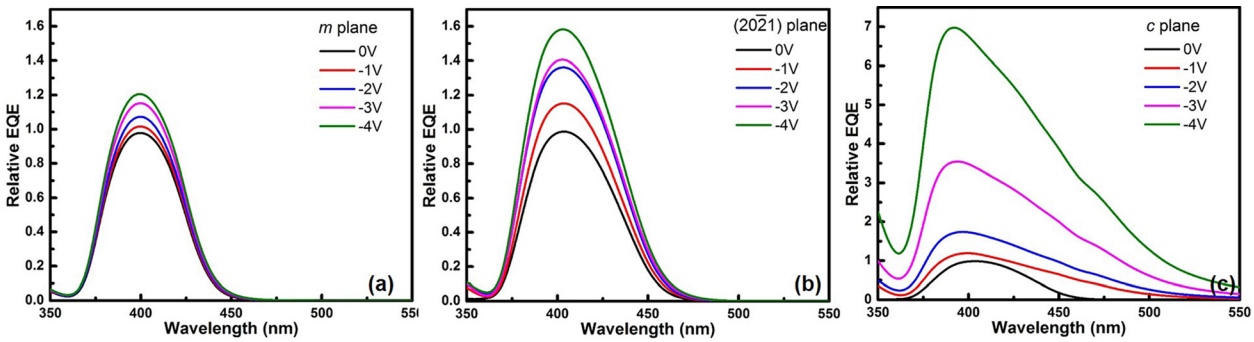

FIG. 3. EQE spectra under different reverse bias conditions of *m*-plane, (20$\bar{2}$1) plane, and *c*-plane InGaN MQW solar cells. Relative EQE was plotted where the EQE spectra from zero bias to −4 V reverse bias was normalized using the peak EQE value under zero condition. Note that the experimental setup used in the biased-EQE measurement is different from that in the previous EQE measurement in Fig. 2. Therefore, the absolute values of EQEs obtained in the biased-EQE experiment differ from the EQE results in Fig. 2.

in the QW energy band profile due to the previously mentioned screening effects on the polarization-induced electric field. In contrast, only negligible change was observed in the absorption edge of the nonpolar *m*-plane device.

To further illustrate the difference in polarizations-related effects on nonpolar *m*-plane, and semipolar (20$\bar{2}$1) plane, and polar *c*-plane devices, simulations for InGaN/GaN MQW structures were carried out using the commercial package developed by the STR Group.[37] The potential distributions were calculated by solving the Schrodinger-Poisson equations self-consistently and include strain and polarization effects. The details of the methods can be found in Ref. 32. Figure 4 demonstrates the simulated energy band diagrams for the $In_{0.20}Ga_{0.80}N$/GaN MQW solar cell with 6 nm InGaN QW and 10 nm GaN barrier on the (a) nonpolar *m*-plane, (b) semipolar (20$\bar{2}$1) plane, and (c) polar *c*-plane. Figure 4(d) shows the comparison zoom-in results of a single QW in three structures. For MQWs with 10 nm GaN barriers, tunneling is the dominant carrier transport mechanism in room temperature.[50,51] Based on Wentzel-Kramers-Bruillouin (WKB) approximations, the tunneling lifetime of an electron in a QW is primarily determined by the barrier width and the barrier height and is given by the following equation:[50]

$$\frac{1}{\tau_T} = \frac{n\pi\hbar}{2m^* L_w^2} \exp\left(\int_0^{L_b} -2\sqrt{\frac{2m^*(E_c(x) - E_n)}{\hbar^2}} dx \right), \quad (2)$$

where τ_T is the tunneling lifetime, m^* is the effective masses, L_w is the well thickness, and L_b is the barrier thickness. To better quantify the effective barrier height for tunneling, H_e is defined as $H_e = E_c - E_n$, where E_c is the average values of conduction band minimum of the barrier on the left of the QW and E_n is the nth subband energy of the electron. We take the electron ground state $E_1(n = 1)$ in one QW. Using this method, we calculated H_e for electrons tunneling from the QW for three structures, which are 0.611 eV, 0.455 eV, and 0.410 eV for polar *c*-plane, semipolar (20$\bar{2}$1) plane, and nonpolar *m*-plane, respectively, as illustrated in Fig. 4(d). As the effective barrier height H_e decreases, the tunneling rate increases, leading to better transport and higher collection of photogenerated carriers. The simulation results are consistent with the experiment results where nonpolar *m*-plane solar cells with lowest H_e and polarization-related effects showed the highest collection efficiency and EQE compared to semipolar (20$\bar{2}$1) plane and polar *c*-plane devices. Polarizations in III-nitride materials will therefore have a significant impact on InGaN solar cell performance.

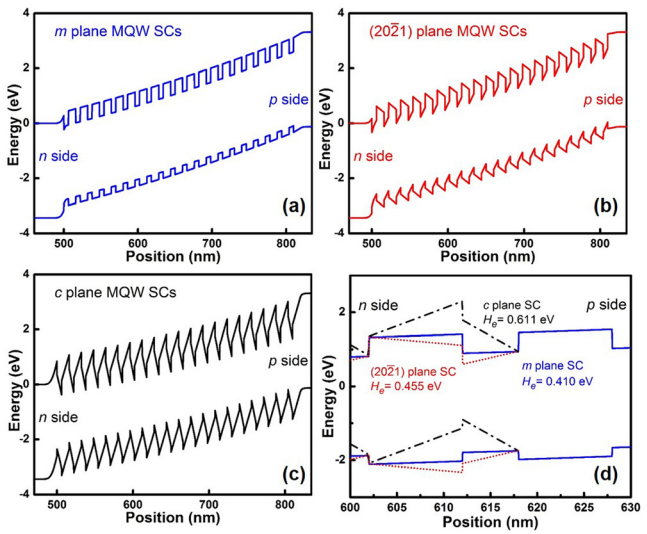

FIG. 4. Schematic energy band diagrams for an $In_{0.20}Ga_{0.80}N$ MQW solar cell with 20 periods of InGaN (6 nm)/GaN (10 nm) MQWs on (a) non-polar *m*-plane, (b) semipolar (20$\bar{2}$1) plane, and (c) polar *c*-plane. (d) shows the comparison zoom-in results of a single QW in three structures and effective barrier height values.

In conclusion, we demonstrate the nonpolar and semipolar InGaN/GaN MQW solar cells based on the nonpolar *m*-plane and semipolar (20$\bar{2}$1) plane bulk GaN substrates, and their PV performance is systematically compared. Nonpolar *m*-plane InGaN/GaN MQW solar cell exhibits the best PV performance across all devices, which is attributed to the improved collection efficiency from the reduced polarization-related effect. The result is further confirmed by bias-dependent EQE measurements and energy band diagram simulations. Our results show the great potential of nonpolar and semipolar devices for future high-efficiency III-nitride solar cells.

This work was supported by an Early Career Faculty grant from NASA's Space Technology Research Grants Program. The authors would like to express sincere gratitude to Mr. Salman Manzoor for the help in transmission and reflection measurements, to Dr. Jacob Becker for the help in IV and EQE measurements, and to Professor Yong-Hang Zhang at Arizona State University for access to his optoelectronics characterization.

[1]C. J. Neufeld, S. C. Cruz, R. M. Farrell, M. Iza, S. Keller, S. Nakamura, S. P. DenBaars, J. S. Speck, and U. K. Mishra, Appl. Phys. Lett. **99**, 071104 (2011).
[2]L. Zhao, T. Detchprohm, and C. Wetzel, Appl. Phys. Lett. **105**, 243903 (2014).
[3]J. J. Williams, H. McFavilen, A. M. Fischer, D. Ding, S. R. Young, E. Vadiee, F. A. Ponce, C. Arena, C. B. Honsberg, and S. M. Goodnick, in *2016 IEEE 43rd Photovoltic Specialists Conference PVSC* (2016), pp. 0193–0195.
[4]Z. Chen, X. Zheng, Z. Li, P. Wang, X. Rong, T. Wang, X. Yang, F. Xu, Z. Qin, W. Ge, B. Shen, and X. Wang, Appl. Phys. Lett. **109**, 062104 (2016).
[5]J. Wu, W. Walukiewicz, K. M. Yu, W. Shan, J. W. A. Iii, E. E. Haller, H. Lu, W. J. Schaff, W. K. Metzger, and S. Kurtz, J. Appl. Phys. **94**, 6477 (2003).
[6]C. J. Neufeld, N. G. Toledo, S. C. Cruz, M. Iza, S. P. DenBaars, and U. K. Mishra, Appl. Phys. Lett. **93**, 143502 (2008).
[7]R.-H. Horng, S.-T. Lin, Y.-L. Tsai, M.-T. Chu, W.-Y. Liao, M.-H. Wu, R.-M. Lin, and Y.-C. Lu, IEEE Electron Device Lett. **30**, 724 (2009).
[8]R. Dahal, J. Li, K. Aryal, J. Y. Lin, and H. X. Jiang, Appl. Phys. Lett. **97**, 073115 (2010).
[9]R. M. Farrell, C. J. Neufeld, S. C. Cruz, J. R. Lang, M. Iza, S. Keller, S. Nakamura, S. P. DenBaars, U. K. Mishra, and J. S. Speck, Appl. Phys. Lett. **98**, 201107 (2011).
[10]N. G. Young, R. M. Farrell, Y. L. Hu, Y. Terao, M. Iza, S. Keller, S. P. DenBaars, S. Nakamura, and J. S. Speck, Appl. Phys. Lett. **103**, 173903 (2013).
[11]N. G. Young, E. E. Perl, R. M. Farrell, M. Iza, S. Keller, J. E. Bowers, S. Nakamura, S. P. DenBaars, and J. S. Speck, Appl. Phys. Lett. **104**, 163902 (2014).
[12]C.-T. Yu, W.-C. Lai, C.-H. Yen, C.-W. Chang, L.-W. Tu, and S.-J. Chang, IEEE Trans. Electron Devices **62**, 1473 (2015).
[13]O. Jani, I. Ferguson, C. Honsberg, and S. Kurtz, Appl. Phys. Lett. **91**, 132117 (2007).
[14]Y. Kuwahara, T. Fujii, T. Sugiyama, D. Iida, Y. Isobe, Y. Fujiyama, Y. Morita, M. Iwaya, T. Takeuchi, S. Kamiyama, I. Akasaki, and H. Amano, Appl. Phys. Express **4**, 021001 (2011).
[15]S. P. DenBaars, D. Feezell, K. Kelchner, S. Pimputkar, C.-C. Pan, C.-C. Yen, S. Tanaka, Y. Zhao, N. Pfaff, R. Farrell, M. Iza, S. Keller, U. Mishra, J. S. Speck, and S. Nakamura, Acta Mater. **61**, 945 (2013).
[16]Y. Kawaguchi, C.-Y. Huang, Y.-R. Wu, Q. Yan, C.-C. Pan, Y. Zhao, S. Tanaka, K. Fujito, D. Feezell, C. G. V. de Walle, S. P. DenBaars, and S. Nakamura, Appl. Phys. Lett. **100**, 231110 (2012).
[17]H. Fu, Z. Lu, and Y. Zhao, AIP Adv. **6**, 065013 (2016).
[18]H. Chen, H. Fu, Z. Lu, X. Huang, and Y. Zhao, Opt. Express **24**, A856 (2016).
[19]L. Sang, M. Liao, Y. Koide, and M. Sumiya, J. Appl. Phys. **117**, 105706 (2015).
[20]Y. Enya, Y. Yoshizumi, T. Kyono, K. Akita, M. Ueno, M. Adachi, T. Sumitomo, S. Tokuyama, T. Ikegami, K. Katayama, and T. Nakamura, Appl. Phys. Express **2**, 082101 (2009).
[21]J. T. Leonard, B. P. Yonkee, D. A. Cohen, L. Megalini, S. Lee, J. S. Speck, S. P. DenBaars, and S. Nakamura, Appl. Phys. Lett. **108**, 031111 (2016).
[22]H. Fu, Z. Lu, X. Huang, H. Chen, and Y. Zhao, J. Appl. Phys. **119**, 174502 (2016).
[23]S. Sakr, E. Giraud, A. Dussaigne, M. Tchernycheva, N. Grandjean, and F. H. Julien, Appl. Phys. Lett. **100**, 181103 (2012).
[24]E. Bellotti, K. Driscoll, T. D. Moustakas, and R. Paiella, Appl. Phys. Lett. **92**, 101112 (2008).
[25]J. S. Speck and D. A. Cohen, in *2015 IEEE High Power Diode Lasers Systems Conference HPD* (2015), pp. 1–2.
[26]R. Dahal, B. Pantha, J. Li, J. Y. Lin, and H. X. Jiang, Appl. Phys. Lett. **94**, 063505 (2009).
[27]Y.-L. Hu, R. M. Farrell, C. J. Neufeld, M. Iza, S. C. Cruz, N. Pfaff, D. Simeonov, S. Keller, S. Nakamura, S. P. DenBaars, U. K. Mishra, and J. S. Speck, Appl. Phys. Lett. **100**, 161101 (2012).
[28]Z. Q. Li, M. Lestradet, Y. G. Xiao, and S. Li, Phys. Status Solidi A **208**, 928 (2011).
[29]J. Y. Chang and Y. K. Kuo, IEEE Electron Device Lett. **32**, 937 (2011).
[30]C. A. M. Fabien, M. Moseley, B. Gunning, W. A. Doolittle, A. M. Fischer, Y. O. Wei, and F. A. Ponce, IEEE J. Photovoltaics **4**, 601 (2014).
[31]C. A. M. Fabien and W. A. Doolittle, Sol. Energy Mater. Sol. Cells **130**, 354 (2014).
[32]Y. Zhao, Q. Yan, C.-Y. Huang, S.-C. Huang, P. S. Hsu, S. Tanaka, C.-C. Pan, Y. Kawaguchi, K. Fujito, C. G. V. de Walle, J. S. Speck, S. P. DenBaars, S. Nakamura, and D. Feezell, Appl. Phys. Lett. **100**, 201108 (2012).
[33]C. J. Neufeld, S. C. Cruz, R. M. Farrell, M. Iza, J. R. Lang, S. Keller, S. Nakamura, S. P. DenBaars, J. S. Speck, and U. K. Mishra, Appl. Phys. Lett. **98**, 243507 (2011).
[34]Y. Zhao, S. Tanaka, Q. Yan, C.-Y. Huang, R. B. Chung, C.-C. Pan, K. Fujito, D. Feezell, C. G. V. de Walle, J. S. Speck, S. P. DenBaars, and S. Nakamura, Appl. Phys. Lett. **99**, 051109 (2011).
[35]D. F. Feezell, J. S. Speck, S. P. DenBaars, and S. Nakamura, J. Disp. Technol. **9**, 190 (2013).
[36]Y. Zhao, F. Wu, C.-Y. Huang, Y. Kawaguchi, S. Tanaka, K. Fujito, J. S. Speck, S. P. DenBaars, and S. Nakamura, Appl. Phys. Lett. **102**, 091905 (2013).
[37]V. F. Mymrin, K. A. Bulashevich, N. I. Podolskaya, I. A. Zhmakin, S. Y. Karpov, and Y. N. Makarov, Phys. Status Solidi C **2**, 2928 (2005).
[38]S. F. Chichibu, A. Uedono, T. Onuma, B. A. Haskell, A. Chakraborty, T. Koyama, P. T. Fini, S. Keller, S. P. DenBaars, J. S. Speck, U. K. Mishra, S. Nakamura, S. Yamaguchi, S. Kamiyama, H. Amano, I. Akasaki, J. Han, and T. Sota, Nat. Mater. **5**, 810 (2006).
[39]S. Chichibu, T. Mizutani, T. Shioda, H. Nakanishi, T. Deguchi, T. Azuhata, T. Sota, and S. Nakamura, Appl. Phys. Lett. **70**, 3440 (1997).
[40]S. John, C. Soukoulis, M. H. Cohen, and E. N. Economou, Phys. Rev. Lett. **57**, 1777 (1986).
[41]Y. Zhao, R. M. Farrell, Y.-R. Wu, and J. S. Speck, Jpn. J. Appl. Phys., Part 1 **53**, 100206 (2014).
[42]X. Huang, H. Fu, H. Chen, Z. Lu, D. Ding, and Y. Zhao, J. Appl. Phys. **119**, 213101 (2016).
[43]R. R. King, D. Bhusari, A. Boca, D. Larrabee, X.-Q. Liu, W. Hong, C. M. Fetzer, D. C. Law, and N. H. Karam, Prog. Photovoltatics: Res. Appl. **19**, 797 (2011).
[44]T. Nakao, T. Fujii, T. Sugiyama, S. Yamamoto, D. Iida, M. Iwaya, T. Takeuchi, S. Kamiyama, I. Akasaki, and H. Amano, Appl. Phys. Express **4**, 101001 (2011).
[45]A. Mukhtarova, S. Valdueza-Felip, L. Redaelli, C. Durand, C. Bougerol, E. Monroy, and J. Eymery, Appl. Phys. Lett. **108**, 161907 (2016).
[46]J. J. Wierer, D. D. Koleske, and S. R. Lee, Appl. Phys. Lett. **100**, 111119 (2012).
[47]L. Redaelli, A. Mukhtarova, A. Ajay, A. Núñez-Cascajero, S. Valdueza-Felip, J. Bleuse, C. Durand, J. Eymery, and E. Monroy, Jpn. J. Appl. Phys., Part 1 **54**, 072302 (2015).
[48]G. J. Lin, K. Y. Lai, C. A. Lin, Y. L. Lai, and J. H. He, IEEE Electron Device Lett. **32**, 1104 (2011).
[49]H. C. Lee, Y. K. Su, W. K. Chuang, J. C. Lin, K. C. Huang, Y. C. Cheng, and K. Jen Chang, Sol. Energy Mater. Sol. Cells **94**, 1259 (2010).
[50]J. R. Lang, N. G. Young, R. M. Farrell, Y.-R. Wu, and J. S. Speck, Appl. Phys. Lett. **101**, 181105 (2012).
[51]S.-B. Choi, J.-P. Shim, D.-M. Kim, H.-I. Jeong, Y.-D. Jho, Y.-H. Song, and D.-S. Lee, Appl. Phys. Lett. **103**, 033901 (2013).